

## From surface to bulk modification: Plasma polymerization of amine-bearing coating by synergic strategy of biomolecule grafting and nitric oxide loading

Tong Yang<sup>a</sup>, Zeyu Du<sup>a</sup>, Hua Qiu<sup>a</sup>, Peng Gao<sup>a</sup>, Xin Zhao<sup>b</sup>, Huaiyu Wang<sup>c</sup>, Qiufen Tu<sup>a</sup>, Kaiqin Xiong<sup>a</sup>, Nan Huang<sup>a</sup>, Zhilu Yang<sup>a,\*</sup>

<sup>a</sup> Key Laboratory of Advanced Technology for Materials of the Education Ministry, School of Materials Science and Engineering, Southwest Jiaotong University, Chengdu, 610031, China

<sup>b</sup> Department of Biomedical Engineering, The Hong Kong Polytechnic University, Hung Hom, Hong Kong, China

<sup>c</sup> Institute of Biomedicine and Biotechnology, Shenzhen Institutes of Advanced Technology, Chinese Academy of Sciences, Shenzhen, 518055, China



### ARTICLE INFO

#### Keywords:

Surface chemistry  
Amine-bearing coating  
Synergic modification  
Biomolecule grafting  
Nitric oxide loading

### ABSTRACT

Integration of two or more biomolecules with synergic and complementary effects on a material surface can help to obtain multi-functions for various biomedical applications. However, the amounts of biomolecules integrated and their physiological functions are compromised due to the limited surface anchoring sites. Herein, we propose a novel concept of film engineering strategy “from surface to bulk synergic modification”. This new concept is realized by employing the surface amine groups of plasma polymerized allylamine (PPAm) film for grafting a molecule e.g., thrombin inhibitor, bivalirudin (BVLD), meanwhile its bulk amine groups is used as a universal depot for storing and releasing therapeutic nitric oxide (NO) gas as supplement to the functions of BVLD. It is demonstrated that such a “from surface to bulk synergic modification” film engineering can impart the modified-substrates with anti-platelet and anti-coagulant dual functions, giving rise to a highly endothelium-mimetic thromboresistant property. We believe that our research provides a very promising strategy to deliver multifunctional surface versatilely that require NO release in combination with other properties, which will find broad biomedical applications in blood-contacting devices, and et al. Moreover, it also provides a brand-new film engineering strategy for tailoring surface multi-functionalities of a wide range of materials.

### 1. Introduction

Recent advances in biomedical devices and their applications mainly rely on the development of surface modification methods [1–4]. Especially, chemical strategies are the preferences for surface modification of biomedical devices due to their energetic effect. As the representatives of surface chemical modifiers, universal coatings delivered by plasma polymerization of organic monomer [5–8] and self-polymerization of catecholamine [9–12], have boosted the great development of applied surface science, engineering and technology. They provide unique advantages to selectively tailor the surface functionalities of a wide range of materials regardless of the inherent chemical compositions and physical characteristics (e.g. stiffness, topology and geometrical shape), and meanwhile the bulk attributes of the materials themselves are not compromised [2,9]. Owing to these merits, these two typical methodologies for attaining material-independent coatings have been widely implemented for the immobilization of

bioactive molecules [5,8–10] and biofunctional organic ad-layers [9] with anti-fouling [6], cell adhesion [7], anti-microbial [11], and wettability controls [12]. Nevertheless, such universal coating strategies show a critical limitation for delivering surface multi-functions. For instance, to create multifunctional surface, the most common method is to employ the surface reactive groups of as-obtained coatings to co-immobilize two or more biomolecules with synergic and complementary effects [13,14]. However, the amounts and physiological functions of target biomolecules is inevitably compromised via surface co-immobilization, which is due to the limited surface space and anchoring sites.

Among the aforementioned coating strategies, plasma polymerization of amine-bearing monomers (e.g. allylamine) (PPAm) and self-polymerization of dopamine (PDA) particularly fascinate many attentions of researchers over past decades. One of the most important reasons is that both PPAm and PDA coatings can provide surface reactive groups (the primary amine groups of PPAm, the catechol/

Peer review under responsibility of KeAi Communications Co., Ltd.

\* Corresponding author.

E-mail address: [zhiluyang1029@swjtu.edu.cn](mailto:zhiluyang1029@swjtu.edu.cn) (Z. Yang).

quinone groups of PDA) to bind with various molecules for optimizing the surface functions [9,10,15–17]. Nevertheless, most of the researchers focus on the surface tailoring but the dominant functional groups in the bulk of coatings are disregarded up to now [18]. Based on previous studies, the secondary amine groups could be utilized to chemically store NO by forming *N*-diazeniumdiolates (NONOates) at high pressure [19]. As the most useful type of NO donors, diazeniumdiolates have aroused widespread interest due to their predictability for generating NO via spontaneous hydrolysis under physiological conditions, e.g. in blood or tissue fluids [20–22]. On the other hand, NO is a liposoluble star gas molecule mainly synthesized by endothelial cells [23]. After winning Nobel prize at 1998, the NO study is still active until now, as it is demonstrated that NO is essential to a wide range of biological systems, including cardiovascular system, nervous system, reproductive system, immune system, as well as cancer development [24–27] with the biological mechanism being further explored.

Here in this study, we present a film engineering strategy from surface molecule grafting to bulk NO loading based on the characteristic merits of PPAm coating. A synergistic modification strategy for integrating the functions of grafted-biomolecule and NO is attained, so as to feature an ideal surface with multi-functions. Under plans, the surface primary amine groups of PPAm coating are used for grafting the anti-coagulant agent bivalirudin (BVLD) and the bulk amine groups are simultaneously utilized to load anti-platelet agent NO as supplement to the functions of BVLD, the resultant coating is denominated as BVLD/NO-PPAm. As is well known, material-triggered thrombus involves two separate yet synergistic events that the adsorbed fibrinogens are activated to form polymerized fibrin networks [28] and the adhered platelets are activated based on cyclic guanosine monophosphate (cGMP)-dependent pathway [29]. The complexity of thrombogenic process determines that single functional agent can hardly meet the exquisite requirement of biomedical devices in direct contact with blood, and the integration of anti-platelet and anti-coagulant agents is a more promising strategy [30–32]. As expected, the BVLD/NO-PPAm coating perfectly combines the anti-platelet and anti-coagulant dual functions of BVLD and NO that is difficult to obtain otherwise. It is believed that this surface to bulk engineering strategy can give a highly endothelium-mimetic thromboresistant property by synergistically grafting BVLD and delivering NO therapy, which will broaden the applications of NO for biomedical and other purposes.

## 2. Materials and methods

### 2.1. Preparation of PPAm, C-F and PPAmF coatings

The PPAm and plasma polymerization of C-F coatings were deposited on 316L stainless steel (SS) substrates using pulsed radio frequency (13.56 MHz) plasma polymerization technique, the detail description of the apparatus can be read elsewhere [33]. In this work, Allylamine (Aam, Purity ≥ 99.0%, Aldrich) monomer was used as precursor to prepare PPAm film, and high-purity argon (Ar) was used as a discharge gas. The Hexafluoroethane (C<sub>2</sub>F<sub>6</sub>, Purity ≥ 99.9%) and acetylene (C<sub>2</sub>H<sub>2</sub>, Purity ≥ 99.0%) were chosen as precursors for fabricating the plasma polymerization of C-F coating.

For the fabrication of PPAm coating, the 316L SS substrates and vacuum chamber were cleaned by Ar (g) plasma for 10 min in advance, and then the PPAm coating was fabricated using 6 sccm of Aam and 0.5 sccm of Ar at a radio frequency (RF) power of 80 W, 25% ( $t_{on} = 250 \mu\text{s}$ ,  $t_{off} = 750 \mu\text{s}$ ) of pulse duty cycle, and 150 V negative bias voltage. After 3 h of deposition, the PPAm with approximate thickness of 300 nm was prepared.

For the fabrication of C-F coating, the mixed precursors of C<sub>2</sub>F<sub>6</sub> (5 sccm) and C<sub>2</sub>H<sub>2</sub> (0.5 sccm) were plasma polymerized at a RF power of 90 W, 80% of pulse duty cycle, and 150 V negative bias voltage [34].

The PPAmF composite coating was obtained by alternative stacking of the PPAm layer with thickness of 30 nm and the C-F layer with

thickness of 20 nm, the final PPAmF coating was composed of 10-layer PPAm film and 9-layer C-F film.

### 2.2. Immobilization of BVLD

To graft BVLD, the samples after PPAmF coating were immersed in a solution containing 1 mg BVLD (2180 Da, Purity ≥ 98%, Chengdu KaiJie Biopharm Co., Ltd.) per 1 mL water-soluble carbodiimide (WSC) solution (pH = 5.6), of which the WSC solution consisted of 9.76 mg/mL of 2-Morpholinoethanesulfonic acid (MES, Purity ≥ 99.0%, Sigma-Aldrich), 0.24 mg/mL of N-hydroxysuccinimide (NHS, Purity ≥ 97.0%, Sigma-Aldrich) and 1 mg/mL of N-(3-dimethylaminopropyl)-N'-ethyl-carbodiimide (EDC, Purity ≥ 99.0%, Sigma-Aldrich). After 12 h of reaction, the BVLD-PPAm specimens were rinsed 3 times with phosphate buffered saline (PBS) and distilled water to remove the physically adsorbed BVLD. Afterwards, the samples were dried and stored in a sealed container.

### 2.3. Loading of NO in PPAmF coating

The NO-loaded substrates were obtained by subjecting the PPAmF-functionalized substrates to a 0.5 M Sodium methoxide (NaOMe) solution at high pressure. The high-pressure reactor was firstly filled with Ar (g) to vent air and then charged with 75 psi NO (Purity ≥ 99.9%) gas. After 3 days of reaction, the modified samples were washed with methanol to remove the physically adsorbed by-products, subsequently dried and stored at –20 °C before use.

### 2.4. ToF-SIMS analysis

The static ToF-SIMS spectra of PPAm coating was determined by using a ToF-SIMS V spectrometer (ION-TOF GmbH, Münster, Germany). Sample was bombarded by 25 kV Bi<sub>3</sub><sup>+</sup> primary ions with a pulsed current of 0.75 pA. The analysis area was 200 μm × 200 μm, and the acquisition time was fixed to 40 s. Thus, an ion dose was less than  $3 \times 10^{11}$  ions cm<sup>−2</sup>, well below the static limit of SIMS conditions. A low-energy flood gun was used to realize Charge compensation, and three measurements at different locations were performed for each specimen. The spectra were corrected prior to extracting ionic strength data using IonSpec software.

### 2.5. GATR-FTIR and XPS analyses

The chemical structures of various coatings were measured by GATR-FTIR (NICOLET5700) and the surface chemical states were tested by XPS (K-Alpha, Thermo Electron, USA). XPS was performed at 12 kV × 15 mA under a pressure of  $2 \times 10^{-7}$  Pa with a monochromatic Al K $\alpha$  (1486.6 eV) X-ray source. The graphitic carbon peak (284.8 eV) was used as a reference for correction.

### 2.6. Hydrophilicity test

The water contact angles (WCA) were measured on of various samples by employing a Krüss GmbH DSA 100 Mk 2 goniometer (Hamburg, Germany), DSA 1.8 software was used to obtain the images of water drop processing.

### 2.7. Quantitative analysis of amine groups in PPAm coating

Trifluoromethyl benzaldehyde (TFBA) and Trifluoroacetic anhydride (TFAA) derivatization methods in combination with XPS were used to determine the concentration of the primary and secondary amine groups [35]. In brief, the PPAm-coated substrates were placed into a reaction chamber and then was evacuated to a pressure of 1 Pa. Subsequently, the TFBA or TFAA was introduced into the chamber for derivatization reaction. After 12 h of reaction, the samples were

examined by XPS, and the concentrations of primary and secondary amine groups were calculated by the formulas reported in the literature [35].

### 2.8. QCM-D real-time monitoring of BVLD immobilization

The amount of BVLD immobilized on the PPAmF coating was monitored in real time by QCM-D (Q-sense AB, Sweden). Firstly, the PPAmF coating was deposited on a quartz wafer (diameter 10 mm, AT-cut, 5 MHz, Au coated) and placed in the flow chamber of QCM-D. Subsequently, the MES buffer solution was flowed into the chamber at a rate of 50  $\mu\text{L}/\text{min}$ . After the fundamental frequency curve was stabilized, the WSC solution containing BVLD (1 mg/mL) was passed at the same flow rate. Ultimately, the chamber was washed thoroughly by PBS solution to remove the BVLD physically adsorbed on sample. The mass of immobilized BVLD was based on frequency shift ( $\Delta f$ ) and calculated through the Sauerbrey equation [36].

### 2.9. Measurement of NO release

A chemiluminescence NO analyzer (NOA, 280i, Boulder) was used to measure NO released from the specimens containing diazeniumdiolates [37]. During the test, the sample was immersed in PBS (pH = 7.4) at 37 °C after calibration of the instrument, and the released NO was transported from the reaction chamber to the analyzer by nitrogen ( $\text{N}_2$ ) until the amount of released NO was below 1 ppb.

### 2.10. Activity of the adsorbed thrombin

The activity of absorbed thrombin was measured by incubating 20  $\mu\text{L}$  of human thrombin solution (2  $\mu\text{g}/\text{mL}$ ) on various samples for 30 min at 37 °C, then 130  $\mu\text{L}$  of 1% Bovine Serum Albumin (BSA dissolved in PBS) was added and incubated for 10 min to avoid nonspecific adsorption. Afterwards, 130  $\mu\text{L}$  of mixed solution was transferred into a 96-well plate and 130  $\mu\text{L}$  of the 2.2 mg/mL chromogenic substrate S-2238(H-D-Phe-Pip-Arg-pNA-2HC1) for thrombin was added to each well. Finally, a microplate reader ( $\mu\text{Quant}$ , Bio-tek instruments Inc.) was used to detect the absorbance at 405 nm.

### 2.11. Platelet adhesion

Platelet rich plasma (PRP) was obtained by centrifuging fresh human whole blood (the central blood station of Chengdu, China) at 1500 rpm for 15 min. 50  $\mu\text{L}$  of fresh PRP was introduced onto each sample and incubated at 37 °C for 30 min. Subsequently, the samples were rinsed 3 times with 0.9 wt% NaCl solution and fixed with 2.5 wt% glutaraldehyde solution for 12 h. After dehydration and dealcoholization, the platelets adhered on the surfaces were observed by SEM (JSM-7001F, JEOL Ltd., Japan).

### 2.12. Fibrinogen (Fg) adsorption and activation

In the test of Fg adsorption, the samples were placed in 24-well plate and incubated by 50  $\mu\text{L}$  of platelet poor plasma (PPP) for 2 h at 37 °C. After rinsing with PBS, 1% of BSA was dropped onto the samples for 30 min and then washed with PBS. In a next step, 20  $\mu\text{L}$  of HRP-labeled mouse anti-human fibrinogen antibody (Sigma-Aldrich) was added onto each sample, incubated for 1 h at 37 °C, and subsequently rinsed with PBS. After the specimens were dried, 100  $\mu\text{L}$  of tetramethylbenzidine (TMB) chromogenic solution was added to each well for 10 min, and then 50  $\mu\text{L}$   $\text{H}_2\text{SO}_4$  (1 M) was used as the stop solution. Finally, a microplate reader was used to determine the absorbance at 450 nm.

The activation of adsorbed Fg was investigated by indirect immunochemistry. Firstly, each sample was incubated with 50  $\mu\text{L}$  of PPP for 2 h at 37 °C. After PBS rinsing, the samples were blocked by 1% BSA for 30 min and washed with PBS. Subsequently, 20  $\mu\text{L}$  of anti-fibrinogen

gamma chain mouse monoclonal antibody (primary antibody) was added and incubated for 1 h at 37 °C. The samples after PBS rinsing were continuously incubated with 20  $\mu\text{L}$  HRP-labeled goat anti-mouse polyclonal antibody (secondary antibody) for 1 h at 37 °C. The stained samples were further washed with PBS, reacted with 100  $\mu\text{L}$  of chromogenic substrate TMB for 10 min, and then 50  $\mu\text{L}$   $\text{H}_2\text{SO}_4$  (1 M) was added to stop the reaction. Finally, a microplate reader was used to determine the absorbance at 450 nm.

### 2.13. Evaluation of ex-vivo antithrombogenicity

To evaluate the antithrombogenic properties of various samples, *ex vivo* blood circulation assay was performed using the New Zealand white rabbit model with arteriovenous (AV) shunt. The animal experiments were conducted in accordance with the Provisions and General Recommendation of Chinese Experimental Animals Administration Legislation, and following all the ethical guidelines. In particular, 6 New Zealand white rabbits (2.5–3.5 kg) were used and the experimental animals were subjected to general anesthesia by the auricular vein injection of pentobarbital sodium (30 mg/mL/Kg). The 316L SS foils ( $15 \times 9 \text{ mm}^2$ ) with or without surface modifications were rolled up and placed inside the extracorporeal catheter, and the catheter was used to connect the carotid artery and vein. After 2 h of blood flow, the circulation was stopped and the circuits were removed from the animals. After PBS (pH 7.4) rinsing, the occlusive rates of the circuits containing test samples were assessed by examining the lumen area. The blood flow rate was tested at the end of circulation and normalized to that before the start of circulation under the same pressure pump condition. The thrombus formed on samples were photographed and weighed, and then fixed with 2.5 wt% glutaraldehyde solution for 12 h. After dehydration, dealcoholization, and critical point drying, all the samples were characterized by SEM.

### 2.14. Statistical analysis

All the quantitative data in this study were presented as mean  $\pm$  standard deviation (SD). The statistical significance of the data was analyzed by SPSS software using one-way analysis of variance (ANOVA). The probability  $p < 0.05$  was considered as statistically significant. All the *in vitro* and *ex vivo* tests were at least triply performed.

## 3. Results and discussion

### 3.1. Preparation of PPAm coating with capacity to load NO

Initially, the amine-bearing PPAm coating is fabricated by pulsed plasma polymerization using the parameters as 6 sccm of allylamine and 0.5 sccm of argon, 5 Pa of system pressure, 80 W of radio frequency (RF) power input, 25% ( $t_{\text{on}} = 250 \mu\text{s}$ ,  $t_{\text{off}} = 750 \mu\text{s}$ ) of pulse duty cycle, and 150 V of negative bias voltage (Fig. 1A). It has been reported that pulsed mode is preferable for the preparation of PPAm coating with regard to the well-retained amine groups of allylamine after polymerization [38]. As widely reported, the PPAm coating is featured with the high degree of cross-linking structure, leading to a robust chemical stability under various conditions [39]. Both grazing incidences attenuated total reflection Fourier transform infrared spectroscopy (GATR-FTIR) and time of flight secondary ion mass spectrometry (ToF-SIMS) are performed to determine the chemical state of our fabricated PPAm coating. The results of GATR-FTIR analysis reveal the features of allylamine ( $\text{H}_2\text{C}=\text{CH}-\text{CH}_2-\text{NH}_2$ ) structure in the PPAm coating, with the peaks at 3350 and 3210  $\text{cm}^{-1}$  attributed to the N-H stretching vibrations, and the peaks at 2925 and 2860  $\text{cm}^{-1}$  attributed to the aliphatic C-H stretching of  $-\text{CH}_2$  (Fig. 1B). In addition, some new functional groups emerge during the process of plasma polymerization [15,40,41], possibly ascribed to the  $\text{C}\equiv\text{N}$ ,  $-\text{C}=\text{N}=\text{O}$  and  $-\text{C}\equiv\text{C}$ - groups at 2180 and

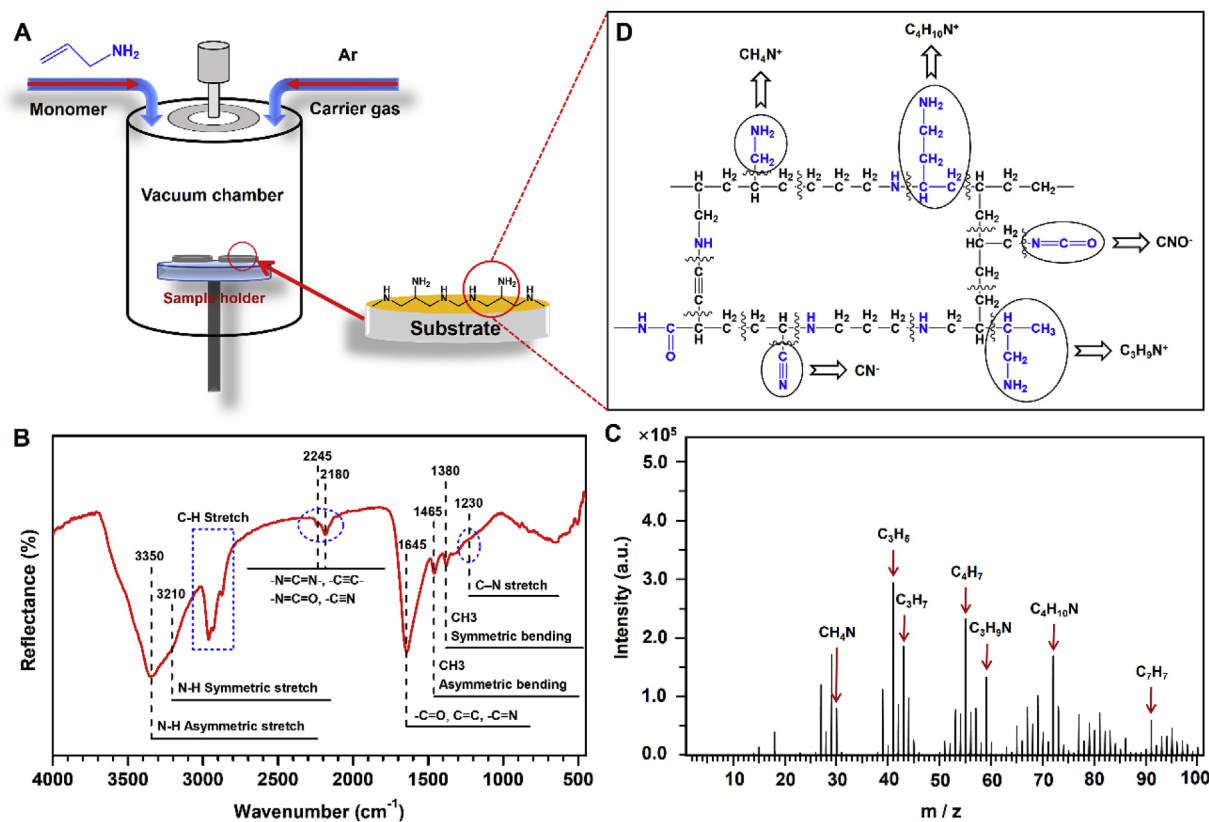


**Fig. 1.** Plasma polymerization of allylamine coating. (A) A schematic illustration of the preparation of PPAm coating by pulsed plasma polymerization of allylamine. (B) GATR-FTIR analysis of the PPAm coating deposited on Au substrate. (C) Tof-SIMS analysis of the PPAm coating deposited on 316L SS substrate. (D) Possible fragments providing secondary ions at  $m/z$  24 ( $\text{CN}^-$ ), 30 ( $\text{CH}_4\text{N}^+$ ), 42 ( $\text{CNO}^-$ ), 59 ( $\text{C}_3\text{H}_9\text{N}^+$ ) and 72 ( $\text{C}_4\text{H}_{10}\text{N}^+$ ) based on the analyses of GATR-FTIR, Tof-SIMS and XPS.

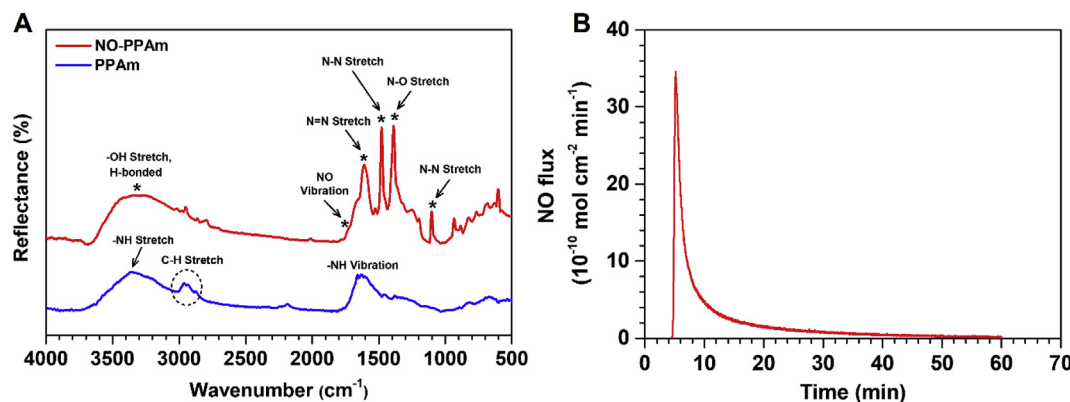


**Fig. 2.** (A) GATR-FTIR spectra of the PPAm coating before and after NO loading. (B) The NO release pattern of PPAm after NO loading.

2245 cm<sup>-1</sup>, and -C=O and C=N groups around 1645 cm<sup>-1</sup>. Further Tof-SIMS analysis indicates that the secondary ions of the most dominant nitrogen contain hydrocarbons at m/z 30 (CH<sub>4</sub>N<sup>+</sup>), 59 (C<sub>3</sub>H<sub>9</sub>N<sup>+</sup>) and 72 (C<sub>4</sub>H<sub>10</sub>N<sup>+</sup>) from the positive spectrum (**Fig. 1C**) and those at m/z 24 (CN<sup>-</sup>) and 42 (CNO<sup>-</sup>) from the negative spectrum (**Supplementary Fig. 1**). To quantitatively examine the primary and secondary amine groups, we performed an analysis of the derivatization reactions in gas phase [35] combined with X-ray photoelectron spectroscopy (XPS), and the corresponding results show that the NH/C ratio (3.1%) exceeds the NH<sub>2</sub>/C ratio (2.1%) (**Supplementary Table 1**), indicating the more secondary amine groups formed in the PPAm than the primary amine groups retention in the PPAm. Based on the aforementioned results of GATR-FTIR, Tof-SIMS and XPS, a possible structure of PPAm coating is illustrated in **Fig. 1D**.

Previous strategies for the loading and release of NO usually involve the use of polymer matrices to encapsulate or physically adsorb the species containing diazeniumdiolates [42,43]. However, most of these existing approaches are defective regarding the poor stability of adsorbed materials in physiological conditions, and the thick coatings ranging from micro-to millimeter are prone to be detached [42–44]. Therefore, the development of a simple and versatile strategy to immobilize NO and release is of great significance. Based on the hypothesis that the PPAm film abundant with amine groups is a versatile and promising loading platform, the NO-storing and release characteristics of PPAm is initially investigated. Firstly, the PPAm coating with a thickness of approximately 300 nm is constructed, and the PPAm-coated substrates are immersed in a sodium methoxide/methyl alcohol mixed solution and subsequently exposed to a high-pressure NO gas

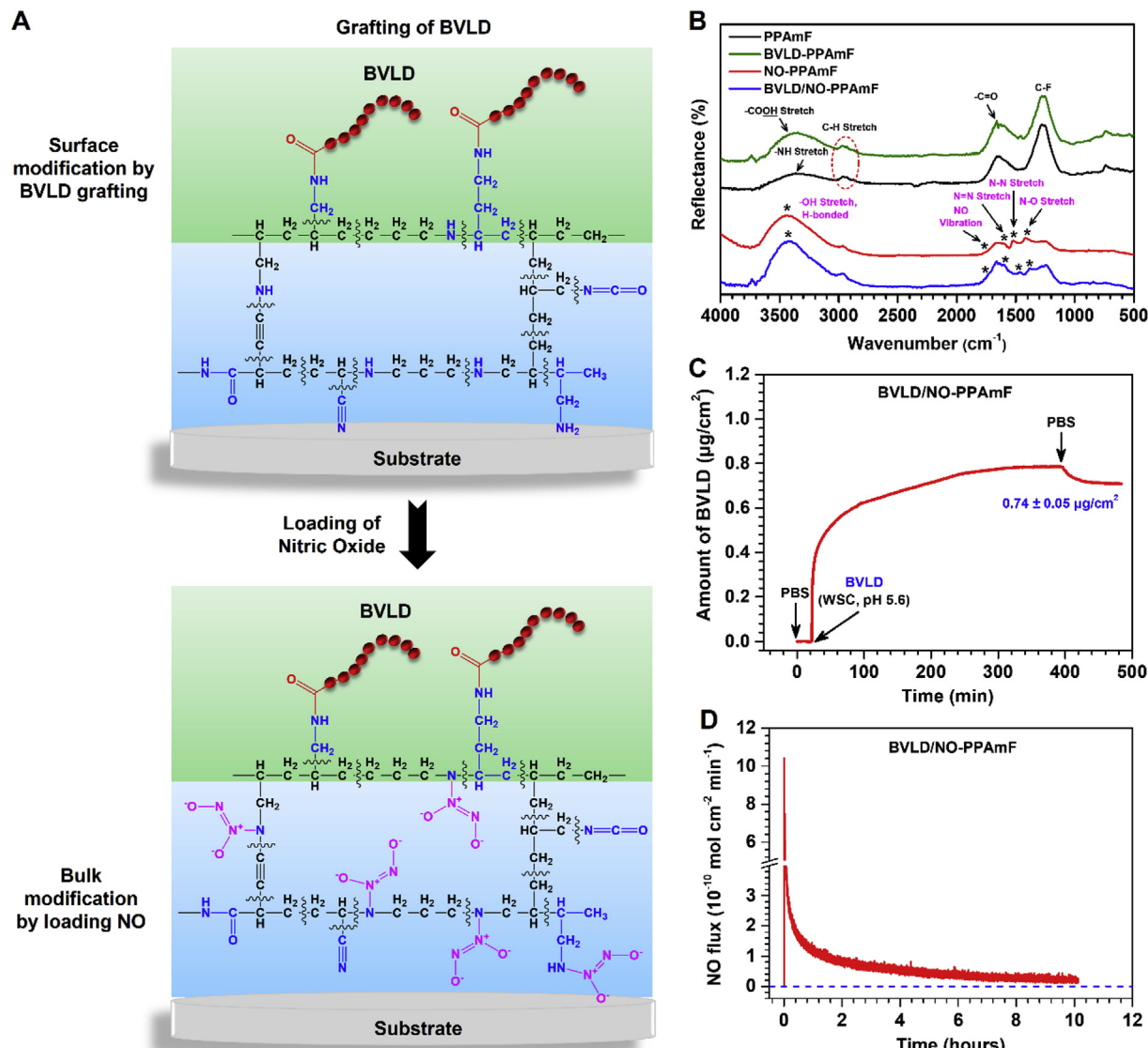


**Fig. 3.** From surface to bulk modification of the PPAmF coating. (A) A schematic illustration of the surface grafting of BLVD and bulk loading NO. (B) GATR-FTIR of the PPAmF, BVLD-PPAmF, NO-PPAmF and BVLD/NO-PPAmF coatings. (C) BVLD grafted on the NO-PPAmF coating real-time monitored by QCM-D ( $n = 4$ ). (D) The NO release pattern of BVLD/NO-PPAmF coating.

atmosphere. To demonstrate the successful loading of NO in the PPAm coating, PPAm coating before and after NO loading is determined using GATR-FTIR. Clearly, the characteristic peaks attributed to the diazeniumdiolate [18], i.e., the NO vibration at  $1735 \text{ cm}^{-1}$ , N=N stretch at  $1610 \text{ cm}^{-1}$ , N-O stretch at  $1386 \text{ cm}^{-1}$ , and the N-N stretch at  $1480 \text{ cm}^{-1}$  are present in the NO-loaded PPAm (NO-PPAm) coatings (Fig. 2A), indicating the successful immobilization of NO. The NO release from functionalized substrates are further tested in phosphate buffered saline (PBS) solution under physiological conditions, using chemiluminescence NO analyzer. As shown in Fig. 2B, a noticeable amount of NO release can be detected from the NO-PPAm coated substrates, confirming the successful storage of NO in the PPAm coating by forming diazeniumdiolates. Taken together, these results demonstrate that the PPAm coating is an efficient platform for NO loading and release.

### 3.2. PPAm coating aiming for synergistic modification from surface to bulk

As a potent anti-platelet agent, NO has been widely used to develop the anticoagulant properties of blood-contacting materials/devices

[45–47]. The anti-platelet activity of NO is ascribed to its capacity to up-regulate the expression of cyclic guanosine monophosphate (cGMP) within platelets. However, material-triggered thrombus involves two separate and synergistic events that including the adsorption and activation of fibrinogen to form polymerized fibrin networks [28], as well as the adhesion and activation of platelets based on cyclic guanosine monophosphate (cGMP)-dependent pathway [29]. Consequently, employing single NO strategy to functionalize blood-contacting materials or biomedical devices with thromboresistant properties but not considering the suppression of fibrinogen adsorption and activation is inadequate *in vivo*.

As is well known, the perfect thromboresistant properties of endothelial cell (EC) layer can be fulfilled by the synergistic effects of anti-platelet agents (e.g., prostacyclin and NO) and anti-coagulants (e.g., heparan sulfates and thrombomodulin). Over the years, many efforts have been dedicated to mimic the high thromboresistance of nature endothelium by integrating these two types of bioactive agents into polymer matrices or co-immobilizing them on material surfaces [30–32,48]. Nonetheless, most of the available methods are subject to either the limited surface anchoring sites for grafting bioactive agents

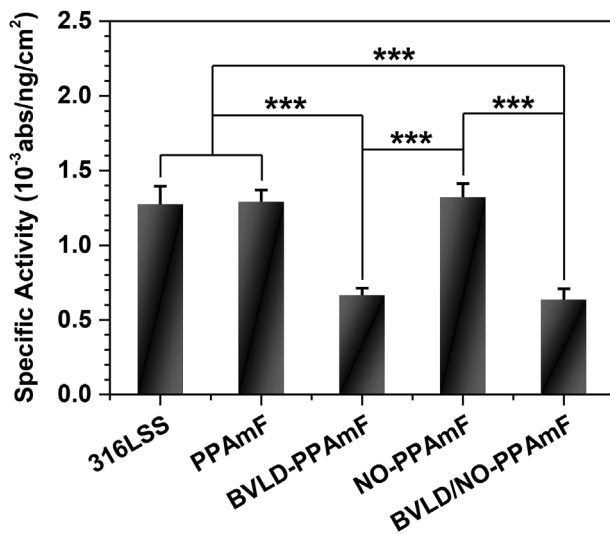


**Fig. 4.** The thrombin quantity ratio between active (absorbance) and adsorbed thrombin ( $\text{ng}/\text{cm}^2$ ) determined on various samples. Data are presented as mean  $\pm$  standard deviation (SD) and analyzed using a one-way ANOVA, \* $p < 0.01$ , \*\* $p < 0.001$ .

or the sophistication of multi-step process that obstructs actual applications.

Herein, we focus on the characteristic merits of PPAm coating including material-independence and the abundance of reactive amine groups to develop a new method for mimicking the perfect thromboresistance of EC layer. In this work, the anti-platelet agent NO and anti-coagulant of direct thrombin inhibitor-bivalirudin (BVLD) are synergistically utilized to develop antithrombogenic surface. In particular, the primary amine groups of PPAm-coated surface are used to covalently immobilize BVLD, and then the BVLD-functionalized PPAm coating immersed in basic solution is subjected to high-pressure NO gas for loading NO. Such a synergistic modification from surface BLDV-grafting to bulk NO-loading is innovative, material-independent, and permits ease of operation. Although PPAm can serve as a NO-loading molecular platform as demonstrated above, it suffers from the poor durability in NO release which limits the practical applications, as the release window is only 1 h by using 300 nm of PPAm coating. Considering that the reason for rapid NO release might be ascribed to the hydrophilic characteristics of PPAm coating [15,16], 9 layers (20 nm of individual layer) of hydrophobic hexafluoroethane (C-F) film (Figs. S2 and S3) are sequentially introduced into 10 layers (30 nm of individual layer) of PPAm to fabricate PPAmF composite coating (Fig. S4), which can resist water invasion into the coating and hence reduce the hydrolytic rate of NONOates. The PPAm and PPAmF film with the same thickness of PPAm (300 nm) are further investigated for the NO release *in vitro*. It is evident that the composite coating strategy can be used to optimize the NO release as expected. Compared with PPAm, the PPAmF coating after loading NO not only reduces the burst NO release, but also prolongs the release time of NO to more than 8 h (Fig. S5).

According to the aforementioned results, the PPAmF-functionalized substrates are subjected to the synergistic modification from surface conjugation of BVLD to bulk NO loading (Fig. 3A). At first, BVLD is immobilized onto the PPAmF coating through a N-hydroxysuccinimide-ethyl(dimethylaminopropyl) carbodiimide (NHS-EDC) coupling reaction. GATR-FTIR analysis demonstrates the presence of C=O stretching band at  $1660 \text{ cm}^{-2}$  in the PPAmF group and the reinforcement of O-H ( $-\text{COOH}$ ) stretching band at  $3420 \text{ cm}^{-2}$  indicates the successful anchor of BVLD (Fig. 3B). The further NO loading leads to the emergence of new peaks at  $1735 \text{ cm}^{-1}$  (NO vibration),  $1596 \text{ cm}^{-1}$  (N=N stretch),  $1466 \text{ cm}^{-1}$  (N-N stretch), and  $1386 \text{ cm}^{-1}$  (N-O stretch) specific to NONOates, which confirms the storage of NO as diazeniumdiolates in

the PPAmF composite coating. The high-resolution N1s spectra corroborates the diazeniumdiolate reaction of BVLD/NO-PPAmF by the presence of new peaks at 402.9 eV (Fig. S6). The hydrophilicity measurements of various substrates also indicate the success of BVLD grafting and NO loading with regard to the significant changes in water contact angles before and after functionalizations (Fig. S7). In a next step, the amount of BVLD immobilized on the PPAmF coating is real-time determined by quartz crystal microbalance with dissipation (QCM-D), and the result shows that a noticeable amount of  $0.74 \pm 0.05 \mu\text{g}/\text{cm}^2$  BVLD is anchored on PPAmF coating (Fig. 3C). This level is comparable to that of PPAm coating (data not shown), indicating that the sequential stacking of C-F and PPAam layers will not compromise the secondary reaction of surface groups for grafting bio-functional molecule. Compared with PPAm, the PPAmF coating after loading NO not only reduces the burst NO release, but also prolongs the release time of NO to more than 8 h (Fig. 3D). Taken together, these findings indicate that the PPAmF coating is quite suitable for the independent but synergistic modification from surface molecule grafting to bulk NO loading, thus can be used to impart biomaterials with designable multi-functions.

### 3.3. Reduced adhesion and activation of platelets and fibrinogen

Previous results have clearly demonstrated that the integration of BVLD and NO on a material can be perfectly realized by the synergistic modification of PPAmF coating strategy from surface to bulk. To further investigate the anti-platelet and anti-coagulant performances of BVLD/NO-PPAmF coating, the tests of *in vitro* platelet adhesion, and fibrinogen (Fg) adsorption and activation are performed. As a synthetic short peptide, BVLD has been well demonstrated for the efficiently inhibitory effects on both circulating and clot-bound thrombin [49]. The bioactivity of BVLD is dominated by both the nitrogen and carbon terminal domains, and the coupling of carboxyl of BVLD may probably lead to a compromise of bioactivity. In this regard, the bioactivity of BVLD/NO-PPAmF coating is investigated by using thrombin inactivation assay [36]. It is clear that the anti-thrombin effect of both the BVLD-PPAmF and BVLD/NO-PPAmF coating is much better than that of 316L SS, PPAmF and NO-PPAmF groups (Fig. 4), implying the good retention of bioactivity after coupling BVLD.

To evaluate the anti-platelet effects of BVLD/NO-PPAmF, the uncoated and coated substrates are exposed to platelet rich plasma (PRP) for 30 min and then determined by scanning electron microscopy (SEM). Evidently, the platelets exhibit serious platelet aggregation and activation on 316L SS and PPAmF, with the highest amounts of adhered platelets on both samples (Fig. 5A). In contrast, the NO-PPAmF coating on 316L SS substrate significantly reduces the platelet adhesion and activation as compared with 316L SS and PPAmF, demonstrating the anti-platelet effects via NO-cGMP mechanism. The BVLD-PPAmF coating also shows substantial inhibitory effects on platelet adhesion and activation, confirming the well-maintained bioactivity of grafted BVLD with the inhibitory effects on thrombin-mediated platelet activation and aggregation [36]. It is noteworthy that the combination of BVLD and NO leads to a further inhibitory effect on both platelet adhesion and activation, as only a few platelets with round and non-activated state are observed on BVLD/NO-PPAmF. According to the statistical analysis, the platelet adhesion/activation determined on BVLD/NO-PPAmF coating is significantly reduced by 2.1/32.5 folds and 1.2/25.2 folds compared to those determined on BVLD-PPAmF and NO-PPAmF coatings (Fig. 5B and C). The synergistic effect of BVLD and NO to suppress platelets is corroborated.

To evaluate the effects on Fg adsorption and activation, enzyme-linked immuno sorbent assay (ELISA) is involved after exposing various samples to platelet poor plasma for 30 min. As respected, both BVLD-PPAmF and BVLD/NO-PPAmF significantly reduce the Fg adsorption (Fig. 5D) and activation (Fig. 5E), indicating the availability of BVLD-functionalization to inhibit Fg through anti-thrombin pathway. It is

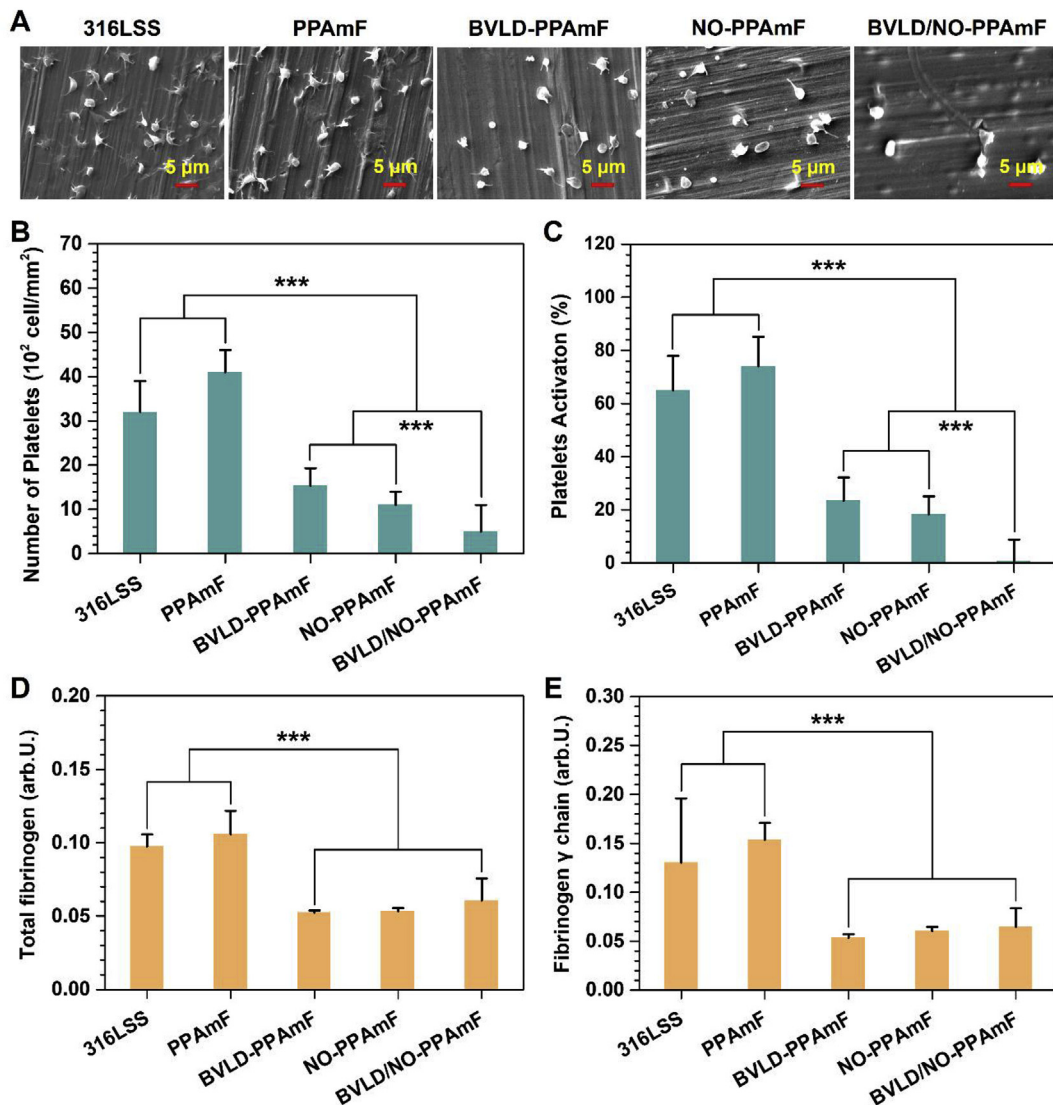


**Fig. 5.** Examinations on the adhesion and activation of platelets and fibrinogen. (A) SEM images of platelets on various substrates after being incubated in PRP for 2 h. (B) The number and (C) the activated rate of adhered platelets. (D) Adsorption and (E) activation of fibrinogen. Data presented as mean  $\pm$  SD ( $n = 4$ ) and analyzed using a one-way ANOVA, \*\*\* $p < 0.001$ .

very interesting that the NO-PPAmF group also shows the inhibitory effects on Fg adsorption and activation [50]. Overall, the previous results demonstrate that the integration of BVLD and NO on a blood-contacting material can arouse anti-platelet and anti-coagulant dual functions.

#### 3.4. Anti-thrombogenicity test by ex vivo blood circulation

To examine whether the BVLD/NO-PPAmF coating is sufficient for resisting the formation of thrombus on a blood-contacting material, an *ex vivo* blood circulation assay is performed using the New Zealand white rabbit model with an arteriovenous (AV) shunt (Fig. 6A). The BVLD/NO-PPAmF coating on 316L SS foils are assembled into the tubing of the circuits (as illustrated in Fig. 6A) and the antithrombogenic properties regarding the occlusive and blood flow rates of the circuits containing the testing samples, as well as the weight of formed thrombus are assessed after 2 h of extracorporeal circulation without any systemic anticoagulation.

The cross profiles of the circuits containing the testing samples reveal that both the bare 316L SS and PPAmF groups cause severe occlusion, whereas the BVLD-PPAmF and NO-PPAmF groups significantly

reduce the occlusion and thrombosis formation. The functionalizations of BVLD and NO are both demonstrated for their efficiency for improving antithrombogenicity *in vivo* (Fig. 6B and C). It is noteworthy that a nearly perfect thromboresistance is achieved by the BVLD/NO-PPAmF coating, as almost no occlusive thrombosis occurs. As shown in Fig. 6D, the thrombuss formed on the bare 316L SS and PPAmF-coated substrate both consist of the fiber network linked with red blood cells and activated platelets. The BVLD-PPAmF coating visibly reduces the formation of fibrin, though some activated platelets are still found on the surface. In the NO-PPAmF group, the platelet adhesion and activation are significantly reduced, but the adherence of polymerized fibrins is still detected. In contrast, the coating with BVLD/NO-PPAmF completely prevents the formation of thrombosis, as very scattered platelets in the nonactivated state are detected on the surface. It demonstrates that perfect antithrombogenicity can be achieved *in vivo* by the synergistic antithrombotic and antiplatelet effects. Further statistical studies reveal that the bare 316L SS induced  $58.7 \pm 3.9\%$  of occlusion (Fig. 6E), and  $64.1 \pm 3.9$  mg of thrombus formation (Fig. 6F), whereas the BVLD-PPAmF and NO-PPAmF coatings reduce the occlusion rate to  $10.5 \pm 1.0$  and  $7.3 \pm 1.8\%$ , and reduce the thrombus formation values to  $4.9 \pm 3.5$  and  $3.7 \pm 1.8$  mg

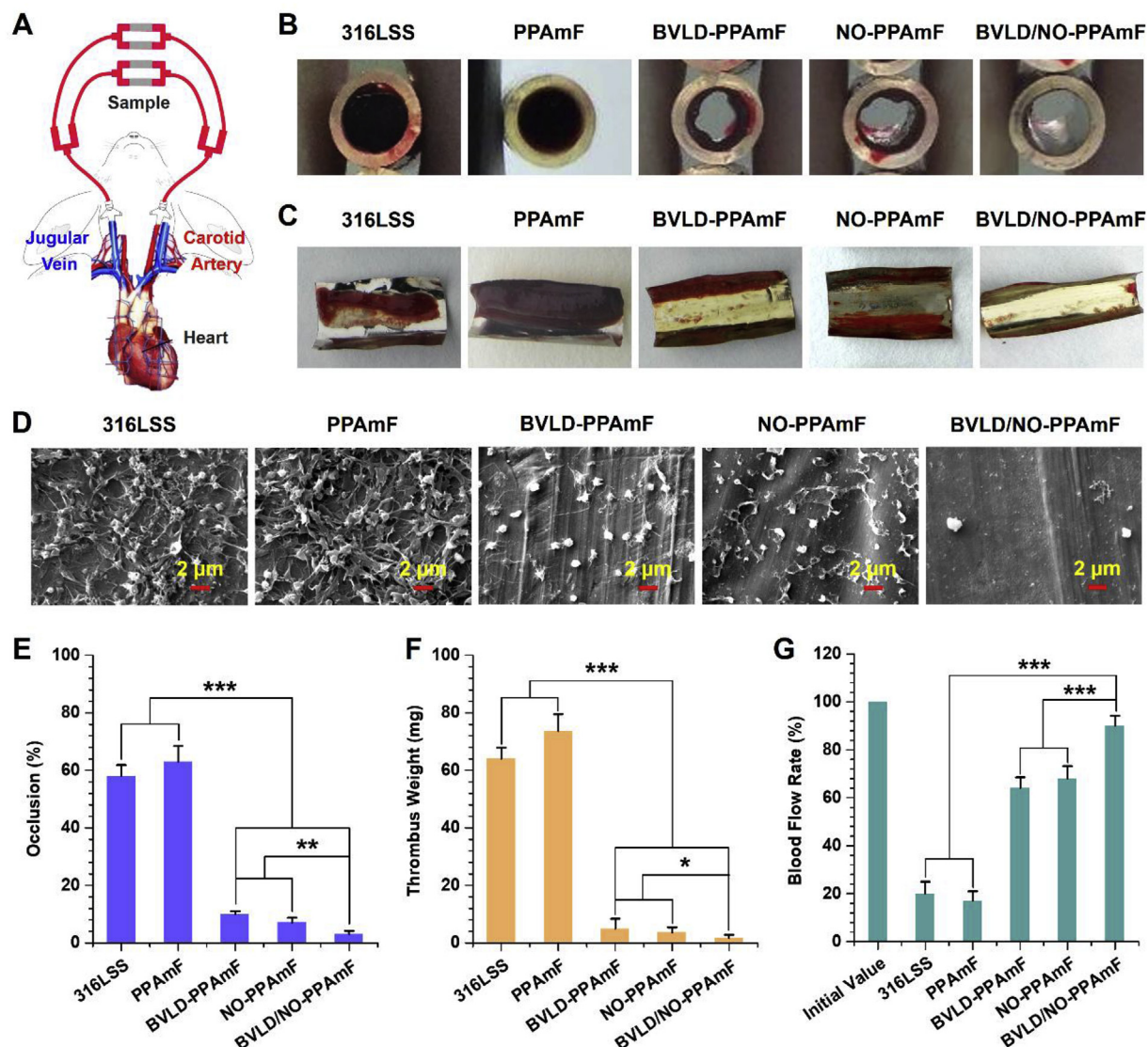


**Fig. 6.** *Ex vivo* thrombogenicity. (A) Schematic of the New Zealand white rabbit model with arteriovenous shunt. (B) Cross sectional images of various samples after 2 h of blood circulation. (C) Photographs of the formed thrombus. (D) The thrombus components evaluated by SEM. (E) Occlusion rates. (F) Weight of thrombus. (G) Retention of blood flow rate. Data are expressed as mean  $\pm$  SD ( $n = 4$ ) and analyzed using a one-way ANOVA, \* $p < 0.05$ , \*\* $p < 0.01$ , \*\*\* $p < 0.001$ .

respectively. As for the BVLD/NO-PPAmF group, the occlusion rate and thrombus weight are further reduced to  $3.3 \pm 1.2\%$  and  $1.7 \pm 1.2$  mg, which are significantly lower than the values determined from the BVLD-PPAmF and NO-PPAmF groups.

The maintenance of desirable blood flow rate is crucial to the success of cardiovascular surgery. In this study, the blood flow rate of various groups at the end of circulation is normalized to that before the start of circulation under the same pressure pump condition. Due to the highly thromboresistant properties, the BVLD/NO-PPAmF group can maintain  $90.4 \pm 4.2\%$  of the initial blood flow rate after 2 h of extracorporeal circulation, which is much higher than that of BVLD-PPAmF group ( $64.2 \pm 4.5\%$ ) and NO-PPAmF group ( $68.7 \pm 5.2\%$ ), not to mention that of uncoated 316L SS ( $20.3 \pm 4.7\%$ ) and PPAmF group ( $16.83 \pm 4.4\%$ ) (Fig. 6G). The above findings indicate the great potential of our engineering strategy “from surface to bulk synergistic modification” to tailor the surface functionalities of blood-contacting materials/devices and meet the high requirements of antithrombogenicity.

#### 4. Conclusion

In summary, a film engineering strategy from surface to bulk modification is proposed in this study by employing the surface amine groups of amine-bearing film for immobilizing bioactive molecule, and the bulk amine groups of film is subsequently used to load NO. By surface grafting thrombin inhibitor BLVD and bulk loading therapeutic gas NO, the anti-platelet and anti-coagulant dual functions can be simultaneously achieved on a blood-contacting material to combat thrombogenicity. The sequential and alternative stacking of hydrophobic C-F and hydrophilic PPAm nano-layers to form PPAmF composite coating can circumvent NO burst release and significantly extend the release time of NO, without compromise the surface graft of biomolecules. Overall, our studies demonstrate a general strategy to synergistically integrate NO therapy and bioactive molecules to develop multi-functions. It is our belief that such a film engineering strategy from surface to bulk modification, may inspire the surface functionalization of other blood-contacting materials and provide new insights into the design of biomedical devices for cardiovascular applications.

## Declaration of competing interest

The authors declare that they have no known competing financial interests or personal relationships that could have appeared to influence the work reported in this paper.

## Acknowledgments

We would like to thank Analytical and Testing Center of Southwest Jiaotong University for the test of SEM. This work was supported by the National Natural Science Foundation of China (Project 31570957), the National Key Research and Development Program of China (2017YFB0702504), International Cooperation Project by Science and Technology Department of Sichuan Province (2019YFH0103) and Applied Basic Research Project funded by Sichuan Provincial Science and Technology Department (2017JY0296).

## Appendix A. Supplementary data

Supplementary data to this article can be found online at <https://doi.org/10.1016/j.bioactmat.2019.12.006>.

## References

- [1] D.Y. Ryu, K. Shin, E. Drockenmuller, C.J. Hawker, T.P. Russell, A generalized approach to the modification of solid surfaces, *Science* 308 (5719) (2005) 236–239.
- [2] Q. Wei, R. Haag, Universal polymer coatings and their representative biomedical applications, *Mater. Horiz.* 2 (6) (2015) 567–577.
- [3] A.M. Cocilite, R.M. Howden, D.C. Borrelli, C.D. Petruzzok, R. Yang, J.L. Yague, A. Ugru, N. Chen, S. Lee, W.J. Jo, A. Liu, X. Wang, K.K. Gleason, 25th anniversary article: CVD polymers: a new paradigm for surface modification and device fabrication, *Adv. Mater.* 25 (38) (2013) 5392–5423.
- [4] H. Ejima, J.J. Richardson, K. Liang, J.P. Best, M.P. van Koeverden, G.K. Such, J. Cui, F. Caruso, One-step assembly of coordination complexes for versatile film and particle engineering, *Science* 341 (6142) (2013) 154–157.
- [5] K.S. Siew, L. Britcher, S. Kumar, H.J. Griesser, Plasma methods for the generation of chemically reactive surfaces for biomolecule immobilization and cell colonization - a review, *Plasma Process. Polym.* 3 (6–7) (2006) 392–418.
- [6] M.-Y. Tsai, Y.-C. Chen, T.-J. Lin, Y.-C. Hsu, C.-Y. Lin, R.-H. Yuan, J. Yu, M.-S. Teng, M. Hirtz, M.H.-C. Chen, C.-H. Chang, H.-Y. Chen, Vapor-based multicomponent coatings for antifouling and biofunctional synergic modifications, *Adv. Funct. Mater.* 24 (16) (2014) 2281–2287.
- [7] S.L. Sanborn, G. Murugesan, R.E. Marchant, K. Kottke-Marchant, Endothelial cell formation of focal adhesions on hydrophilic plasma polymers, *Biomaterials* 23 (1) (2002) 1–8.
- [8] F. Khelifa, S. Ershov, Y. Habibi, R. Snyders, P. Dubois, Free-radical-induced grafting from plasma polymer surfaces, *Chem. Rev.* 116 (6) (2016) 3975–4005.
- [9] H. Lee, S.M. Dellatore, W.M. Miller, P.B. Messersmith, Mussel-inspired surface chemistry for multifunctional coatings, *Science* 318 (5849) (2007) 426–430.
- [10] H. Lee, J. Rho, P.B. Messersmith, Facile conjugation of biomolecules onto surfaces via mussel adhesive protein inspired coatings, *Adv. Mater.* 21 (4) (2009) 431–434.
- [11] S.M. Kang, N.S. Hwang, J. Yeom, S.Y. Park, P.B. Messersmith, I.S. Choi, R. Langer, D.G. Anderson, H. Lee, One-step multipurpose surface functionalization by adhesive catecholamine, *Adv. Funct. Mater.* 22 (14) (2012) 2949–2955.
- [12] S.M. Kang, I. You, W.K. Cho, H.K. Shon, T.G. Lee, I.S. Choi, J.M. Karp, H. Lee, One-step modification of superhydrophobic surfaces by a mussel-inspired polymer coating, *Angew. Chem. Int. Ed. Engl.* 49 (49) (2010) 9401–9404.
- [13] F. Bally, K. Cheng, H. Nandividya, X. Deng, A.M. Ross, A. Panades, J. Lahann, Co-immobilization of biomolecules on ultrathin reactive chemical vapor deposition coatings using multiple click chemistry strategies, *ACS Appl. Mater. Interfaces* 5 (19) (2013) 9262–9268.
- [14] Y.B. Lee, Y.M. Shin, J.H. Lee, I. Jun, J.K. Kang, J.C. Park, H. Shin, Polydopamine-mediated immobilization of multiple bioactive molecules for the development of functional vascular graft materials, *Biomaterials* 33 (33) (2012) 8343–8352.
- [15] J.R. Hollohan, T. Wydeven, Synthesis of reverse osmosis membranes by plasma polymerization of allylamine, *Science* 179 (4072) (1973) 500–501.
- [16] D.A. Puleo, R.A. Kissling, M.S. Sheu, A technique to immobilize bioactive proteins, including bone morphogenetic protein-4 (BMP-4), on titanium alloy, *Biomaterials* 23 (9) (2002) 2079–2087.
- [17] H. Qiu, P. Qi, J. Liu, Y. Yang, X. Tan, Y. Xiao, M.F. Maitz, N. Huang, Z. Yang, Biomimetic engineering endothelium-like coating on cardiovascular stent through heparin and nitric oxide-generating compound synergistic modification strategy, *Biomaterials* 207 (2019) 10–22.
- [18] S. Hong, J. Kim, Y.S. Na, J. Park, S. Kim, K. Singha, G.I. Im, D.K. Han, W.J. Kim, H. Lee, Poly(norepinephrine): ultrasmooth material-independent surface chemistry and nano-depot for nitric oxide, *Angew. Chem. Int. Ed. Engl.* 52 (35) (2013) 9187–9191.
- [19] N.A. Stasko, M.H. Schoenfisch, Dendrimers as a scaffold for nitric oxide release, *J. Am. Chem. Soc.* 128 (25) (2006) 8265–8271.
- [20] M.C. Jen, M.C. Serrano, R. van Lith, G.A. Ameer, Polymer-based nitric oxide therapies: recent insights for biomedical applications, *Adv. Funct. Mater.* 22 (2) (2012) 239–260.
- [21] N. Naghavi, A. de Mel, O.S. Alavijeh, B.G. Cousins, A.M. Seifalian, Nitric oxide donors for cardiovascular implant applications, *Small* 9 (1) (2013) 22–35.
- [22] J.A. Hrabie, L.K. Keefer, Chemistry of the nitric oxide-releasing diazeniumdiolate (“Nitrosohydroxylamine”) functional group and its oxygen-substituted derivatives, *Chem. Rev.* 102 (4) (2002) 1135–1154.
- [23] F. Murad, Discovery of some of the biological effects of nitric oxide and its role in cell signaling, *Biosci. Rep.* 24 (4–5) (2004) 452–474.
- [24] J. Hou, Y. Pan, D. Zhu, Y. Fan, G. Feng, Y. Wei, H. Wang, K. Qin, T. Zhao, Q. Yang, Y. Zhu, Y. Che, Y. Liu, J. Cheng, D. Kong, P.G. Wang, J. Shen, Q. Zhao, Targeted delivery of nitric oxide via a ‘bump-and-hole’-based enzyme-prodrug pair, *Nat. Chem. Biol.* 15 (2) (2019) 151–160.
- [25] B.B. Mishra, V.A. Rathinam, G.W. Martens, A.J. Martinot, H. Kornfeld, K.A. Fitzgerald, C.M. Sasse, Nitric oxide controls the immunopathology of tuberculosis by inhibiting NLRP3 inflammasome-dependent processing of IL-1 $\beta$ , *Nat. Immunol.* 14 (1) (2013) 52–60.
- [26] W. Xu, L.Z. Liu, M. Loizidou, M. Ahmed, I.G. Charles, The role of nitric oxide in cancer, *Cell Res.* 12 (5–6) (2002) 311–320.
- [27] A.W. Carpenter, M.H. Schoenfisch, Nitric oxide release: part II. Therapeutic applications, *Chem. Soc. Rev.* 41 (10) (2012) 3742–3752.
- [28] E.W. Davie, K. Fujikawa, W. Kisiel, The coagulation cascade: initiation, maintenance, and regulation, *Biochemistry* 30 (43) (1991) 10363–10370.
- [29] P.-Y. Cheung, E. Salas, R. Schulz, M.W. Radomski, Nitric oxide and platelet function: implications for neonatology, *Semin. Perinatol.* 21 (5) (1997) 409–417.
- [30] B. Wu, B. Gerlitz, B.W. Grinnell, M.E. Meyerhoff, Polymeric coatings that mimic the endothelium: combining nitric oxide release with surface-bound active thrombomodulin and heparin, *Biomaterials* 28 (28) (2007) 4047–4055.
- [31] D.J. Suchyta, H. Handa, M.E. Meyerhoff, A nitric oxide-releasing heparin conjugate for delivery of a combined antiplatelet/anticoagulant agent, *Mol. Pharm.* 11 (2) (2014) 645–650.
- [32] T.C. Major, E.J. Brisbois, A.M. Jones, M.E. Zanetti, G.M. Annich, R.H. Bartlett, H. Handa, The effect of a polyurethane coating incorporating both a thrombin inhibitor and nitric oxide on hemocompatibility in extracorporeal circulation, *Biomaterials* 35 (26) (2014) 7271–7285.
- [33] Z. Yang, X. Lei, J. Wang, R. Luo, T. He, H. Sun, N. Huang, A novel technique toward bipolar films containing alternating nano-layers of allylamine and acrylic acid plasma polymers for biomedical application, *Plasma Process. Polym.* 8 (3) (2011) 208–214.
- [34] D. Yu, Q. Hua, X. Mou, Z. Dou, N. Zhou, Q. Guo, N. Lyu, L. Lu, Z. Yang, N. Huang, One-pot but Two-step Vapor-Based Amine- and Fluorine-Bearing Dual-Layer Coating for Improving Anti-corrosion and Biocompatibility of Magnesium Alloy, *ACS Biomaterials Science & Engineering*, 2019.
- [35] A. Choukourou, H. Biederman, D. Slavinska, M. Trchova, A. Hollander, The influence of pulse parameters on film composition during pulsed plasma polymerization of diamino-cyclohexane, *Surf. Coat. Technol.* 174–175 (2003) 863–866.
- [36] Z. Yang, Q. Tu, M.F. Maitz, S. Zhou, J. Wang, N. Huang, Direct thrombin inhibitor-bivalirudin functionalized plasma polymerized allylamine coating for improved biocompatibility of vascular devices, *Biomaterials* 33 (32) (2012) 7959–7971.
- [37] P.N. Coneski, M.H. Schoenfisch, Nitric oxide release: part III. Measurement and reporting, *Chem. Soc. Rev.* 41 (10) (2012) 3753–3758.
- [38] P. Hamerli, T. Weigel, T. Groth, D. Paul, Surface properties of and cell adhesion onto allylamine-plasma-coated polyethylenterephthalat membranes, *Biomaterials* 24 (22) (2003) 3989–3999.
- [39] Z. Zhang, Q. Chen, W. Knoll, R. Förch, Effect of aqueous solution on functional plasma polymerized films, *Surf. Coat. Technol.* 174–175 (2003) 588–590.
- [40] B. Finke, F. Luethen, K. Schroeder, P.D. Mueller, C. Bergemann, M. Frant, A. Ohl, B.J. Nebe, The effect of positively charged plasma polymerization on initial osteoblastic focal adhesion on titanium surfaces, *Biomaterials* 28 (30) (2007) 4521–4534.
- [41] F. Truica-Marasescu, M.R. Wertheimer, Nitrogen-rich plasma-polymer films for biomedical applications, *Plasma Process. Polym.* 5 (1) (2008) 44–57.
- [42] H. Zhang, G.M. Annich, J. Miskulin, K. Osterholzer, S.I. Merz, R.H. Bartlett, M.E. Meyerhoff, Nitric oxide releasing silicone rubbers with improved blood compatibility: preparation, characterization, and in vivo evaluation, *Biomaterials* 23 (6) (2002) 1485–1494.
- [43] A.B. Seabra, M.G. De Oliveira, Poly(vinyl alcohol) and poly(vinyl pyrrolidone) blended films for local nitric oxide release, *Biomaterials* 25 (17) (2004) 3773–3782.
- [44] Z. Zhou, M.E. Meyerhoff, Preparation and characterization of polymeric coatings with combined nitric oxide release and immobilized active heparin, *Biomaterials* 26 (33) (2005) 6506–6517.
- [45] T.C. Major, D.O. Brant, M.M. Reynolds, R.H. Bartlett, M.E. Meyerhoff, H. Handa, G.M. Annich, The attenuation of platelet and monocyte activation in a rabbit model of extracorporeal circulation by a nitric oxide releasing polymer, *Biomaterials* 31 (10) (2010) 2736–2745.
- [46] Q. Zhao, J. Zhang, L. Song, Q. Ji, Y. Yao, Y. Cui, J. Shen, P.G. Wang, D. Kong, Polysaccharide-based biomaterials with on-demand nitric oxide releasing property regulated by enzyme catalysis, *Biomaterials* 34 (33) (2013) 8450–8458.
- [47] A. de Mel, F. Murad, A.M. Seifalian, Nitric oxide: a guardian for vascular grafts? *Chem. Rev.* 111 (9) (2011) 5742–5767.
- [48] R. Simon-Walker, R. Romero, J.M. Staver, Y. Zang, M.M. Reynolds, K.C. Popat, M.J. Kipper, Glycocalyx-Inspired nitric oxide-releasing surfaces reduce platelet adhesion and activation on titanium, *ACS Biomater. Sci. Eng.* 3 (1) (2017) 68–77.
- [49] S.X. Anand, M.C. Kim, M. Kamran, S.K. Sharma, A.S. Kini, J. Fareed, D.A. Hoppensteadt, F. Carbon, E. Cavusoglu, D. Varon, J.F. Viles-Gonzalez, J.J. Badimon, J.D. Marmur, Comparison of platelet function and morphology in patients undergoing percutaneous coronary intervention receiving bivalirudin versus unfractionated heparin versus clopidogrel pretreatment and bivalirudin, *Am. J. Cardiol.* 100 (3) (2007) 417–424.
- [50] M.A. Elnaggar, S.H. Seo, S. Gobaa, K.S. Lim, I.H. Bae, M.H. Jeong, D.K. Han, Y.K. Joung, Nitric oxide releasing coronary stent: a new approach using layer-by-layer coating and liposomal encapsulation, *Small* 12 (43) (2016) 6012–6023.